analytical chemistry

pubs.acs.org/ac Article

Rapid Discrimination of Extracellular Vesicles by Shape Distribution Analysis

Sou Ryuzaki,* Takao Yasui, Makusu Tsutsui, Kazumichi Yokota, Yuki Komoto, Piyawan Paisrisarn, Noritada Kaji, Daisuke Ito, Kaoru Tamada, Takahiro Ochiya, Masateru Taniguchi, Yoshinobu Baba,* and Tomoji Kawai*

Cite This: *Anal. Chem.* 2021, 93, 7037−7044 Read Online

ACCESS | Metrics & More | Article Recommendations | Supporting Information

ABSTRACT: A rapid and simple cancer detection method independent of cancer type is an important technology for cancer diagnosis. Although the expression profiles of biological molecules contained in cancer cell-derived extracellular vesicles (EVs) are considered candidates for discrimination indexes to identify any cancerous cells in the body, it takes a certain amount of time to examine these expression profiles. Here, we report the shape distributions of EVs suspended in a solution and the potential of these distributions as a discrimination index to discriminate cancer cells. Distribution analysis is achieved by low-aspect-ratio nanopore devices that enable us to rapidly analyze EV shapes individually in solution, and the present results reveal a dependence of EV shape distribution on the type of cells (cultured liver, breast, and colorectal cancer cells and cultured normal breast cells) secreting EVs. The findings in this study provide realizability and experimental basis for a simple method to discriminate several types of cancerous cells based on rapid analyses of EV shape distributions.

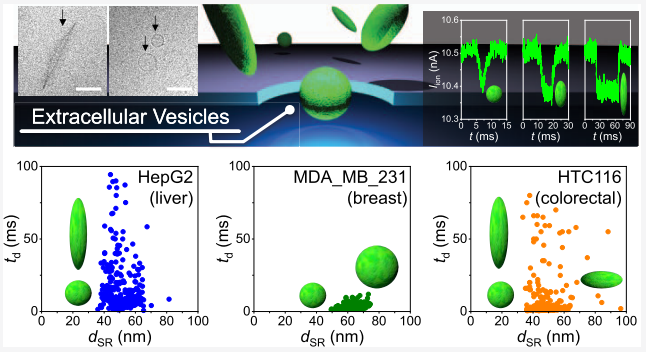

Early detection of cancer tumors in the body is well known to be one of the most important factors for the radical cure of cancer.[1−3] However, it is difficult to detect all types of tumors at an early stage because detection methods differ among the types of cancer, and some of the methods require invasive and painful medical procedures. Thus, a universal method enabling the detection of all types of cancer tumors in the body without invasive procedures, i.e., via a simple and rapid procedure independent of the cancer type, has been widely sought after and researched worldwide.[4] Cell-derived extracellular vesicles (EVs), especially 50−200 nm, called exosomes, are increasingly recognized as the main biomarker for such a universal method.[5−10] EVs originate from the endosomal system and are present in biological fluids. Notably, they contain biological molecules such as proteins, lipids, and nucleic acids that carry information about the cells that secrete them.[11−15] In addition, genetic materials contained in EVs and exosomal integrins are involved in intercellular communications and cancer metastases, respectively.[16−18] This suggests that some kind of cancerous tumor in the body can be detected and identified by analyzing the biological molecules in cancer-cell-derived EVs present in biological fluids. Indeed, microRNAs in lung, pancreas, liver, bladder, and prostate cancer cell-derived EVs have been reported to be discriminable.[15] However, it takes a certain amount of time to profile the expression of these biological molecules. Therefore, investigating rapid and simple identification methods for EVs is a key approach for realizing a universal method for cancer detection, screening, and diagnosis. Here, we report the shape distribution of cultured cell-derived EVs suspended in solution and the potential of the distributions as a discrimination index to identify EVs. There are no previous reports of a correlation between the EV shape distribution and the cells secreting the EVs, although a large number of publications have reported transmission electron microscopic (TEM) images of many kinds of EVs.[19] This is mainly due to the difficulty of measuring the shape of nanomaterials in solution. We recently developed low-aspect-ratio nanopore devices that enable the rapid shape analysis of single particles suspended in solution.[20,21] Here, a low-aspect ratio is defined as the ratio of the nanopore thickness (L) to its diameter (D). The shapes of suspended EVs can thus be measured individually using this simple nanopore-sensing method; subsequently, a shape

Received: January 19, 2021
Accepted: April 19, 2021
Published: April 28, 2021

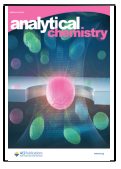

https://doi.org/10.1021/acs.analchem.1c00258
Anal. Chem. 2021, 93, 7037−7044

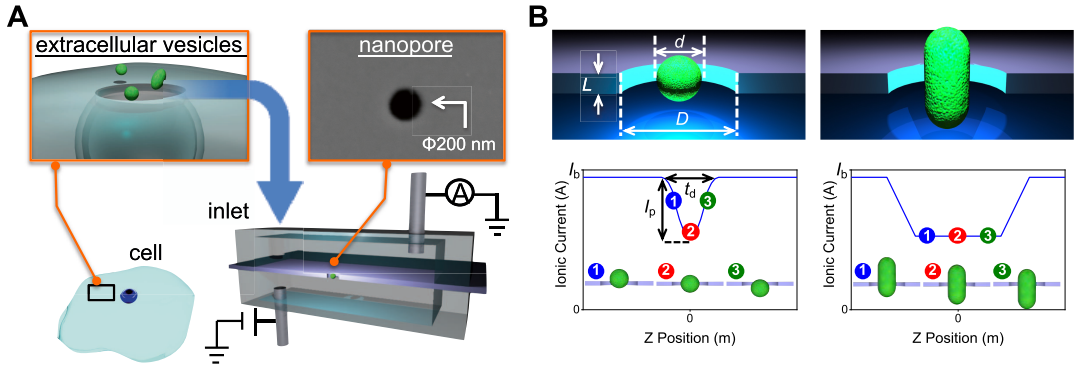

Figure 1. Schematic illustrations of the shape distribution analysis of extracellular vesicles suspended in solution. (A) Schematic illustration of a nanopore device. The cell-derived EVs dispersed in an electrolyte solution were measured using a 35-nm-thick (L) and 200-nm-diameter (D) Si_3N_4 nanopore device. The inset picture is an SEM image of the nanopore. Both sides of a nanopore in a Si_3N_4 substrate were sealed with PDMS sheets including microfluid channels. Here, the figure illustrates a cross-sectional device. (B) Schematic illustration of the dependence of the ionic current blockade, i.e., resistive pulse, on EV shapes. EVs, whose diameter (d) is smaller than D, can pass through a nanopore by electrophoresis, resulting in blockages of the ionic current flowing through a nanopore, i.e., ionic current blockades. The ionic current blockades are characterized by intensity (I_p), duration time (t_d), and shape; the larger diameter and longer shape EVs fundamentally cause the larger I_p and longer t_d, respectively. For example, spherical and rod nanoparticles cause spike-shaped and square resistive pulses, respectively. As d can be estimated from I_p, shape distributions of EVs can be analyzed by $I_p(d)$–t_d plots.

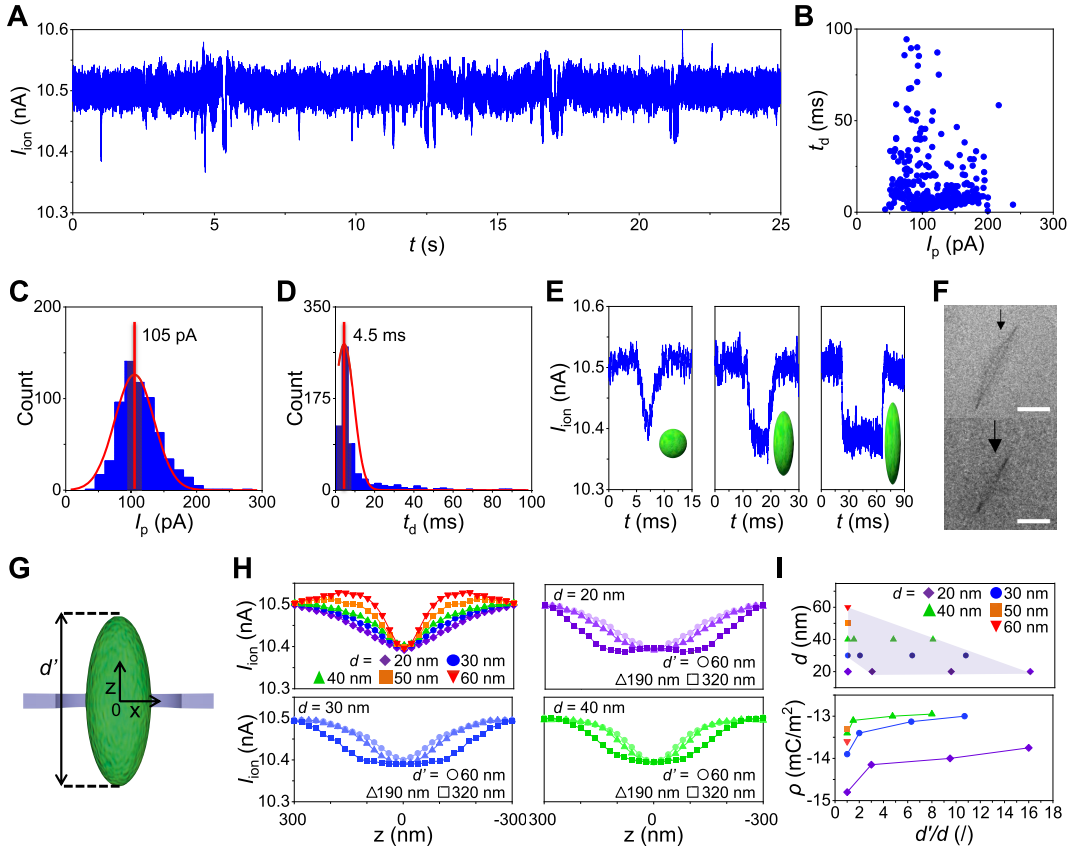

Figure 2. Quantitative shape distribution analysis of HepG2-EVs in a solution. (A) A part of ionic current with some blocking currents due to HepG2-EVs passing through a nanopore. (B) I_p–t_d plots extracted from the blocking currents due to HepG2-EVs translocation events. The number of measured EVs (n) is 649. (C) I_p histogram of the resistive pulses extracted from the blocking currents. (D) t_d and I_p histograms from the resistive pulses. (E) Some of the most typical blocking currents with I_p = 105 pA and t_d = 4.5 ms and others with longer t_d. (F) TEM images of HepG2-EVs extracted by the ultracentrifugation process (indicated by the arrow). The scale bar corresponds to 100 nm. (G) Schematic illustration of an ellipsoidal EV with definitions of the x-axis, z-axis, and d', which correspond to the diameter of long axes. (H) z–I_{ion} plots with I_p = 105 pA of spherical EVs simulated by the MP model (upper left) for each diameter of d = 20 nm (purple diamond), 30 nm (blue circle), 40 nm (green triangle), 50 nm (orange square), and 60 nm (red inverted triangle). Simulated z–I_{ion} plots of ellipsoidal EVs with d = 20 nm (upper right), 30 nm (lower left), and 40 nm (lower right). Here, the dependences of the plots on d' = 60 nm (circle), 190 nm (triangle), and 320 nm (square) are simulated. (I) d'/d–d (upper) and d'/d–ρ (lower) plots causing 105-pA-I_p. The colored area in the upper figure potentially indicates a region of ellipsoidal EVs causing 105-pA-I_p.

https://doi.org/10.1021/acs.analchem.1c00258
Anal. Chem. 2021, 93, 7037−7044

distribution is obtained rapidly by statistically analyzing each shape.

In this study, we measured the shape distributions of EVs derived from the cultured liver (HepG2), breast (MDA_MB_231), and colorectal (HTC116) cancer cells and cultured normal breast cells (MCF10A) using low-aspect-ratio nanopore devices and discussed the discriminability of the distributions. In nanopore devices, analytes dispersed in an electrolyte solution can pass through an orifice by electrophoresis, resulting in an ionic current blockade for each analyte translocation event (Figure 1A).[22,23] Since blocking currents generally depend on the volume of an analyte inside a nanopore, we can estimate shape information, such as the diameter (d), the continuous cross-sectional volume, and the approximate length, of an analyte from the peak intensity (I_p), shape, and duration time (t_d) of blocking currents, respectively (Figure 1B).

EXPERIMENTAL SECTION

Fabrication of Nanopore Devices. Nanopores in a thin Si_3N_4 membrane with thickness-to-diameter aspect ratios of 0.175 (= 35/200 nm) were fabricated by electron-beam lithography. The details are described in our previous works.[20] For the ionic current measurements, poly(dimethylsiloxane) (PDMS) sheets including microfluid channels, inlet, and outlet were adhered onto both sides of the substrate.

Measurement System and Analysis Method of Ionic Currents. For EV detection, an electrophoretic field V_b = 0.8 V was applied to the pore utilizing two Ag/AgCl electrodes at both PDMS sheets to detect a sufficient number of EVs. In the cases where V_b was less than 0.8 V, it was difficult to detect EVs efficiently (Figure S1). The ionic current I_{ion} was monitored at 1 MHz, and the 1 MHz ionic current−time data were compressed to 100 kHz for analyses of the blocking currents. Each blocking current was automatically found in the compressed current−time data by an algorithm programmed by LabVIEW; subsequently, the peak intensity (I_p) and duration time (t_d) of the blocking currents were extracted to examine $I_p(d_{SR})-t_d$ plots. All processes of the present analyses were performed within a few minutes.

Preparations of Extracellular Vesicles. Human liver (HepG2, ATCC), breast (MDA-MB-231, ATCC), and colorectal (HTC116, ATCC) cancer cells were cultured in DMEM (1195-065, Thermo Fisher Scientific Inc.) with 10% exosome-depleted FBS (EXO-FBS-250A-1, System Biosciences, LLC) without the addition of any antibiotics and filtered with a 0.22 μm filter (8020-500, AGC Inc., Japan). In each passage, 2×10^6 cells were seeded into 15 mL of the cell medium and cultured in an incubator (MCO-5ACUV-PJ, Panasonic Corporation, Japan) at 37 °C and 5% CO_2. After 2 days, the cell medium was removed from the culture flask and filtered with a 0.22 μm filter (SLGS033SB, Merck Millipore, Ireland). Twenty milliliters of the filtered medium was pipetted into ultracentrifuge tubes and ultracentrifuged at 110 000g for 80 min; this method is one of the most fairly efficient protocols to separate EVs with high recovery and low specificity.[24] After the first ultracentrifugation, the supernatant was aspirated, the pellet was washed with 10 mL PBS, pH 7.2 (20012-027, Thermo Fisher Scientific Inc.), and the sample was ultracentrifuged for the second time under similar conditions as the first ultracentrifugation. After the second ultracentrifugation, the supernatant was aspirated, and the EV pellet was resuspended in 1 mL of TE buffer. The isolated EV was stored at −80 °C. Each EV solution was backed to room temperature, and its EV concentration was adjusted to 1/100 in TE buffer (1×10^8 particles/mL) before the measurements.

Multiphysics Model Calculation. We set up the multiphysical model to evaluate the I_p dependences on the shape, size, and surface charge density of EVs. All calculations were performed using COMSOL Multiphysics (Figure S2).[25]

RESULTS AND DISCUSSION

Quantitative Shape Distribution Analysis for EVs in Solution. The shape and shape distribution of HepG2-EVs in the TE buffer were evaluated quantitatively. For the ionic current (I_{ion}) measurements using a Si_3N_4 nanopore with L = 35 nm and D = 200 nm, resistive blocking currents due to the EV translocations were detected with a baseline current (I_b) of 10.5 nA (Figure 2A), and the I_p-t_d plot extracted from all of the resistive pulses shows a wide t_d distribution in 1−100 ms (Figure 2B). Some of the most typical resistive pulses based on each I_p and t_d histogram, which is monomodally distributed at approximately I_p = 105 pA and t_d = 4.5 ms (Figure 2C,D), show spike and square pulses with short and long t_d, respectively (Figure 2E). It is reasonable to assign spike pulses with short t_d to spherical EVs,[20] while square pulses with long t_d generally indicate translocation events of analytes with longitudinally extended shapes, such as ellipsoidal particles, or the temporal trapping of an analyte inside a nanopore by electroosmotic flow.[26] In the case of trapping, the noise level of the ionic current should be increased because a trapped analyte causes additional current fluctuation due to Brownian motion (Figure S3). As all of the observed square pulses have the same S/N ratio as that of the baseline current, these pulses with long t_d (Figure 2E) potentially indicate translocation events of ellipsoidal EVs. Indeed, many ellipsoidal HepG2-EVs were observed by TEM (indicated by the arrow), as shown in Figure 2F.

The multiphysics (MP) model simulation constructed from hydromechanics, electromagnetics, and ionic transport theory also reproduced the dependence of a resistive pulse on the EV shapes (Figure 2G−I).[27,28] In the present MP simulations, the blocking currents at each z-position of the EVs were calculated with the assumption that the EVs were translocating on the center axis (x = 0) of a nanopore. Therefore, the $z-I_{ion}$ plots shown in Figure 2H represent resistive pulses due to the EV translocations in uniform motion. However, the plots cannot trace the experimental results perfectly, meaning that nonuniform motions of the EVs would occur due to the electroosmotic flow inside a nanopore because the electroosmotic flow running in the opposite direction from the EV translocations is the strongest at approximately z = 0 in the present MP simulation (Figure S4). The translocation speed is thus decelerated when the EV approaches the pore center, resulting in relatively short rise and fall times in a pulse signal. For spike pulses, 105-pA-I_p was found to be caused by spherical EVs of d = 20, 30, 40, 50, and 60 nm with surface charge densities (ρ) of −14.8, −13.9, −13.4, −13.3, and −13.6 mC/m^2, respectively (upper left in Figure 2H). Here, the surface charge density ρ and resistive pulse shape are important factors in determining the EV diameters. The value of ρ should be greater than −14 mC/m^2 because the ζ potential of the EVs is reported to be approximately −30 mV, which corresponds to more than −14 mC/m^2 according to theoretical equations for typical buffer solutions (1−20 mM).[29,30] The ionic current at the rising (falling) edges of the simulated pulses tended to

https://doi.org/10.1021/acs.analchem.1c00258
Anal. Chem. 2021, 93, 7037−7044

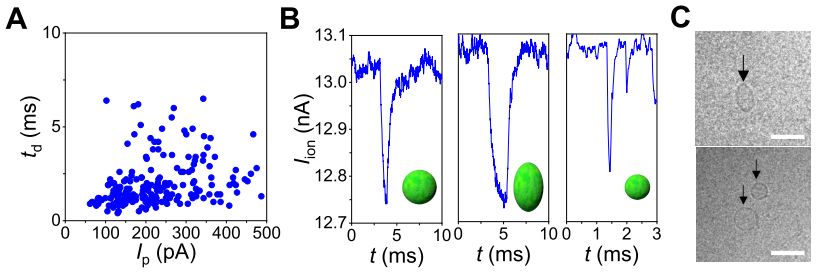

Figure 3. Shape analysis of HepG2-EVs extracted by ExoQuick. (A) I_p−t_d plots of EVs (n = 212). The distribution characteristics are different from those of the same EVs extracted by the ultracentrifugation processes as shown in Figure 2b. (B) Resistive pulses of the blocking current due to translocations of HepG2-EVs extracted by ExoQuick. These signal shapes indicate spherical and almost spherical EVs. (C) TEM images of HepG2-EVs extracted by ExoQuick (indicated by the arrow). The scale bar corresponds to 100 nm.

increase with d and exceeded the baseline current at d = 60 nm (red inverted triangle), which was slightly observed in the present experiments. These facts thus suggest that the minimum and maximum diameters of spherical HepG2-EVs are ca. 30 and 60 nm, respectively. On the other hand, ellipsoidal EVs with $d'/d > 8$ were found to cause square pulses, similar to the experimental results (Figure 2E), and the diameters should be in the range of 20−40 nm according to the same reasoning as the spherical EVs considering the surface charge density and the rising (falling) edge behavior. Here, d' denotes the long-axis length of the EVs (Figure 2G). In the case of ellipsoidal EVs ($d'/d > 1$), there are various combinations of parameters (d'/d, d, and ρ) that result in resistive pulses with 105-pA-I_p. Although it is difficult to simulate all the combinations, HepG2-EVs with parameters in the colored area shown in Figure 2I would cause such pulses because the data at d = 60 with d'/d = 1, d = 30 with d'/d = 1, d = 20 with d'/d = 3, and d = 20 with d'/d = 16 are the threshold points for 105-pA-I_p. Furthermore, the present MP model simulations revealed dependences of square pulse shapes on the parameters d'/d, d, and ρ (Figure 2H). A simulated square pulse for an EV with d'/d = 16, d = 20 nm, and $\rho = -13.75$ mC/m^2 shows a gradual dip surrounding z = 0 (purple square, upper right in Figure 2H), whereas ionic currents achieve the minimum value at z = 0 for EVs with d = 30 and 40 nm (lower right and left in Figure 2H). These results indicate the possibility of realizing more rigorous quantitative analyses for the shape and surface charge density of ellipsoidal EVs from shape information on the resistive pulses. As the experimental results actually show various shapes at the pulse top (center and right in Figure 2E), the analyses would be more rigorous if we could measure the resistive pulses with a much better S/N ratio than that of the present data. In addition, we should discuss the off-axis and rotation effects when considering more rigorous quantitative analyses (Figure S5).[31]

The present results experimentally and theoretically suggest the existence of ellipsoidal HepG2-EVs. However, both TEM-observed and simulated ellipsoidal EVs seem to be artificial shapes and appear as elongated structures compared with other reports about TEM images[19] and shape variations due to the electron field inside nanopores.[32] In addition, the simulated absolute values of the surface charge density $|\rho|$ of the ellipsoidal EVs are lower than those of the spherical EVs (Figure 2I). These facts suggest that some EVs with a spherical or near-spherical original shape could be stretched into ellipsoidal shapes during the ultracentrifugation process. To verify this speculation, we next examined the shape distribution of HepG2-EVs extracted by ExoQuick, which requires no ultracentrifugal force on the EVs. The EVs were collected from 1 mL of cell medium according to the kit (ExoQuick-TC, System Biosciences, Inc.) manufacturer's instruction manual. Here, a nanopore structure with a thickness of 35 nm and a diameter of 300 nm was employed in this experiment because extractions using the relatively mild ExoQuick process potentially resulted in more heterogeneous EV populations, including larger EVs, than ultracentrifugation. Equivalent diameter histograms (d_{ED}) obtained by TEM observations indeed show a larger size population of ExoQuick-extracted EVs (Figure S6). The I_p−t_d plot of the HepG2-EVs extracted by ExoQuick clearly indicates an absence of ellipsoidal EVs (Figure 3A) because of a noticeably narrow t_d distribution compared to the results shown in Figure 2B. TEM images (indicated by the arrow) and each ionic resistive pulse also support the existence of only spherical EV shapes (Figure 3B,C). These results make it possible to conclude that some of the present HepG2-EVs are stretched by ultracentrifugation, meaning that these ellipsoidal EVs are softer particles than spherical EVs. Meanwhile, since the physical properties of EVs were found to depend on the methods of EV extraction, we should examine I_p−t_d plots of HepG2-EVs extracted by other methods and discuss which method is the most appreciated extraction for nanopore sensing to discriminate EVs in the future.

Comparing Shape Distributions of EVs Derived from Three Kinds of Cancer Cells. As the I_p−t_d plots have information about the EV shape distributions, the plots are considered to be a distinctive feature for the discrimination of EVs. Here, we compared three kinds of EVs derived from the liver (HepG2), breast (MDA_MB_231), and colorectal (HTC116) cancer cells. MDA_MB_231-EVs and HTC116-EVs extracted by ultracentrifugation were measured by a 200-nm-diameter nanopore, as were HepG2-EVs. Since I_b and I_p depend on experimental conditions, I_p was normalized to EV diameter by the series-resistant (SR) model to compare the three on the same scale (Figure S7).[20,21] Because the SR model does not account for the surface charge of materials passing through a nanopore and the off-axis effects, the diameters estimated by the model (d_{SR}) are slightly different from the actual diameters (Figure S8). However, this model is commonly utilized for resistive pulse sensors such as the qNano particle analyzer (Meiwafosis Co., Ltd.) as a tool to estimate diameters approximately because of the simple numerical calculation, in contrast to the MP model, which requires computational finite element modeling.[33,34] Gaussian fittings to each d_{SR} histogram show a variance in symmetrical

https://doi.org/10.1021/acs.analchem.1c00258
Anal. Chem. 2021, 93, 7037−7044

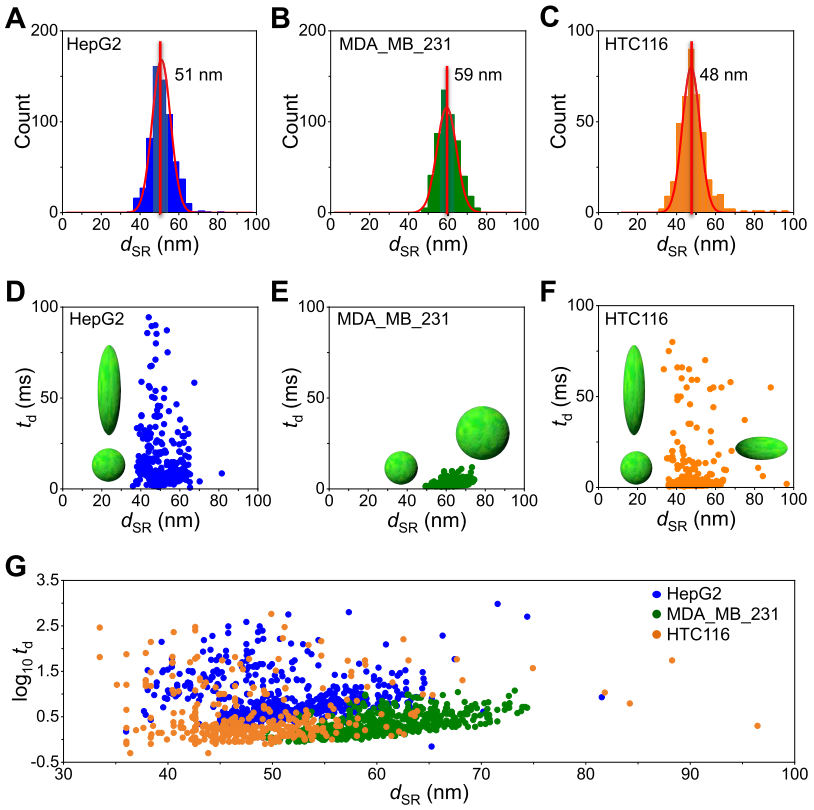

Figure 4. Diameter (d_{SR}) histograms and d_{SR}–t_d plots of three kinds of EVs derived from HepG2, MDA_MB_231, and HTC116 cells. (A–C) Histograms of HepG2- (blue), MDA_MB_231- (green), and HTC116- (orange) EV diameter d_{SR}, which were estimated using the SR model (n = 649, 518, and 391, respectively). The distribution centers are 51, 59, and 48 nm, respectively. (D–F) d_{SR}–t_d plots obtained from each blocking current due to HepG2- (blue), MDA_MB_231- (green), and HTC116- (orange) EV translocation events. (G) d_{SR}–$\log_{10} t_d$ plots of HepG2- (blue), MDA_MB_231- (green), and HTC116- (orange) EV.

monomodal distributions centered at approximately 50–60 nm and relatively narrow d_{SR} distributions (Figure 4A–C). The narrow d_{SR} distribution is assumed to be due to EVs from individual cell lines. In addition, in the case of EVs with small surface charge, such as small EVs called exomere,[36] electrophoretic force on these EVs becomes smaller because of the small surface charge. Therefore, it might be difficult for these EVs to pass through a nanopore if the electrophoretic force is weaker than the electroosmotic flows inside a nanopore that runs in the opposite direction from the EV translocations, resulting in relatively narrow d_{SR} distributions with few small EVs. In addition, as the estimated diameters are relatively smaller than in other reports, the EVs might be compressed by the electric field inside a nanopore.[32] Indeed, for a 35-nm-thick nanopore, the electric field inside a nanopore is estimated to be 26 kV/cm by the MP model simulation, which is comparable to the electric field causing deformation of a liposome passing through a nanopore (Figure S9).[32] However, the d_{SR} distribution is independent of V_b for the present nanopore devices (Figure S9). Because, in general, independence of d_{SR} from V_b indicates that the electric field causes small effects on the deformation,[32] the EV shape distributions are inferred to be unaltered largely by the effect in this study. Although one of the reasons for this independence of d_{SR} from V_b could be because the Young's moduli of EVs are reported to be higher than those of liposomes,[35,36] the detailed impacts of the electric field on the EV shape remain to be solved. In a comparison among the three distributions, it is not certain that the 10 nm differences in d_{SR} distributions are meaningful information for discriminating and/or identifying EVs. On the other hand, each d_{SR}–t_d plot shows significant differences in the distributions (Figure 4D–F). The differences in d_{SR}–t_d plots are much more noticeable in d_{SR}–$\log_{10} t_d$ plots (Figure 4G), and each p-value of Welch's t-test between HepG2 and MDA_MB_231, MDA_MB_231 and HTC116, and HepG2 and HTC116 shows less than 0.05, meaning that these d_{SR}–t_d plots have statistically different distributions with each other. For the MDA_MB_231-EV plot, most of the EVs appear to have a spherical structure, as the plots show a narrow distribution of t_d (1–10 ms), in contrast to the HepG2-EVs and a linear relation between d_{SR} and t_d (Figure 4E). This is a typical d_{SR}–t_d distribution of spherical particles.[20] In the case of HTC116-EVs, spherical EVs are predominant, although there are a few ellipsoidal EVs (Figure 4F). It is of interest to note that many of the HTC116-EVs pass through a nanopore within 5 ms regardless of diameter. This could be due to translocations by EVs turning sideways to a nanopore, i.e., the long axis of ellipsoidal EVs is perpendicular to the direction of EV translocations. These perpendicular ellipsoidal EV translocations cause larger I_p (d_{SR}) and shorter t_d than parallel ellipsoidal EV translocations in principle (Figure S5). Since the nanopore diameter is 200 nm, the long-axis length of most ellipsoidal HTC116-EVs is less than 200 nm, whereas there are a lot of ellipsoidal HepG2-EVs with long-axis lengths of more than 200 nm because many plots with long t_d and small d_{SR} are confirmed in the d_{SR}–t_d distribution (Figure 4D). This conclusion regarding the size and shape of the EVs is reasonable with respect to the results discussed in Figure 2.

https://doi.org/10.1021/acs.analchem.1c00258
Anal. Chem. 2021, 93, 7037–7044

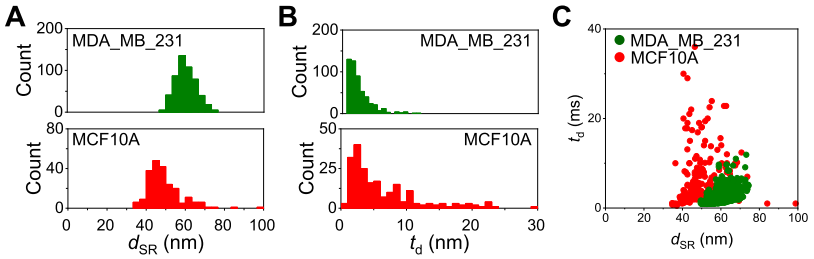

Figure 5. Evaluating the potential of the EV shape distributions as a discrimination index to detect cancerous cells. (A) d_{SR} histograms of MDA_MB_231- (green) and MCF10A- (red) EVs (n = 518 and 219, respectively). (B) t_d histograms of MDA_MB_231- (green) and MCF10A- (red) EVs. (C) Comparison of d_{SR}−t_d plots between MDA_MB_231- (green) and MCF10A- (red) EVs. The d_{SR}−t_d plots show significant difference between the two EVs, indicating a different shape distribution.

The differences among the three plots are attributed to the differences in the EV shape distribution. However, the d_{SR}−t_d plots could also suggest variability in the EV stiffness because the ellipsoidal EVs seem to be caused by the ultracentrifugation process, indicating that the present ultracentrifugation plays a key role in differentiating EV shape distributions. The EV stiffness is anticipated to depend on the components of the EV membranes,[37−40] and the correlation between d_{SR}−t_d plots and membrane components would be important information to understand EVs in further studies.

Comparing Shape Distributions of EVs Derived from Cancer and Normal Cells. Here, we discuss the potential of EV shape distributions as a discrimination index to identify cancerous cells. The d_{SR}−t_d plots of MDA_MB_231-EVs were compared with those from normal breast cells (MCF10A) to evaluate the ability to discriminate between the EVs from cancerous and normal cells. The results related to MDA_MB_231-EVs shown in Figure 5 are the same data as in Figure 4. For the d_{SR} histograms of MCF10A-EVs, the distributions overlapped in a range of 40−70 nm as well as the other EVs (Figure 5A). In addition, each duration time histogram mutually shows almost the same tendency, although some MCF10A-EVs pass through a nanopore with a relatively long duration of ca. 10 ms (Figure 5B). On the other hand, each d_{SR}−t_d plot is distributed in different ranges with distinct tendencies, meaning a different shape distribution between the two types of EVs (Figure 5C). Indeed, the p-values of Welch's t-test between MDA_MB_231 and MCF10A is 1.0×10^{-14}.

These results suggest the possibility of discriminating cancerous cells by measuring EV shape distributions. Because the present study examines only 4 types of shape distributions of cultured cell-derived EVs, we cannot conclude that the d_{SR}−t_d plot of EVs in biological fluids is a novel index to find and/or identify cancerous cells in the body. However, the results presented here suggest that it is worthwhile to undertake a statistical analysis of d_{SR}−t_d plots of various EVs from cultured cells and biological fluids to discuss the availability of EV shape distributions as the index of a rapid and simple cancer detection method. In fact, d_{SR}−t_d plots of EVs extracted from the blood of breast cancer patients and people in normal health resulted in different distributions (Figure S10).

CONCLUSIONS

In the case of the present EVs (HepG2, MDA_MB_231, HTC116, and MCF10A) derived from cultured cells, low-aspect-ratio solid-state nanopore devices found that the shape distribution of EVs suspended in solution depended on the type of cells secreting the EVs. Because some EVs were stretched by ultracentrifugation for EV extractions that resulted in more noticeable differences in EV shape distribution, extraction by ultracentrifugation could be important for the present EV discrimination method. Although this study examined EVs derived from cultured cells, these findings would advance a rapid and simple cancer detection method via biological fluid tests. Measuring more various types of EVs will provide us with the more accurate potential of the EV shape distributions as an index for cancer detection, screening, and diagnosis. In addition, these various EV shape distributions, i.e., d_{SR}−t_d plots of both real and cultured samples, would be utilized as training data for AI (Figure S10). The big data sets will play a key role in translating d_{SR}−t_d plots into medical information and greatly contribute to understanding EVs from the perspectives of both fundamental biology and clinical screening for the diagnosis of cancer.

ASSOCIATED CONTENT

Supporting Information

The Supporting Information is available free of charge at https://pubs.acs.org/doi/10.1021/acs.analchem.1c00258.

Ionic current at V_b = 0.5−1.0 V; model for the multiphysics simulations; effect of Brownian motion on a noise level of ionic current; dynamics of an EV passing through a nanopore; off-axis and rotation effects; equivalent diameters of HepG2-EVs extracted by ultracentrifugation and ExoQuick; the series-resistant model; accuracy of the series resistance model for nanoparticles; dependence of d_{SR} of HepG2-EVs on V_b and the electric field inside a nanopore; d_{SR}−t_d plots of the EVs extracted from real blood of people in normal health (NH) and breast cancer (BC) patients (PDF)

AUTHOR INFORMATION

Corresponding Authors

Sou Ryuzaki − *Institute for Materials Chemistry and Engineering, Kyushu University, Fukuoka 812-0395, Japan; PRESTO, Japan Science and Technology Agency (JST), Saitama 332-0012, Japan;* orcid.org/0000-0002-3288-642X; Email: ryuzaki@ms.ifoc.kyushu-u.ac.jp

Yoshinobu Baba − *Department of Biomolecular Engineering, Nagoya University, Nagoya 464-8603, Japan;* Email: babaymtt@chembio.nagoya-u.ac.jp

Tomoji Kawai − *The Institute of Scientific and Industrial Research, Osaka University, Osaka 567-0047, Japan;* Email: kawai@sanken.osaka-u.ac.jp

https://doi.org/10.1021/acs.analchem.1c00258
Anal. Chem. 2021, 93, 7037−7044

Authors

Takao Yasui − *PRESTO, Japan Science and Technology Agency (JST), Saitama 332-0012, Japan; Department of Biomolecular Engineering, Nagoya University, Nagoya 464-8603, Japan;* orcid.org/0000-0003-0333-3559

Makusu Tsutsui − *The Institute of Scientific and Industrial Research, Osaka University, Osaka 567-0047, Japan;* orcid.org/0000-0002-4552-1163

Kazumichi Yokota − *The Institute of Scientific and Industrial Research, Osaka University, Osaka 567-0047, Japan*

Yuki Komoto − *The Institute of Scientific and Industrial Research, Osaka University, Osaka 567-0047, Japan;* orcid.org/0000-0002-9004-3797

Piyawan Paisrisarn − *Department of Biomolecular Engineering, Nagoya University, Nagoya 464-8603, Japan*

Noritada Kaji − *Department of Applied Chemistry, Kyushu University, Fukuoka 819-0395, Japan;* orcid.org/0000-0002-9828-873X

Daisuke Ito − *Institute for Integrated Radiation and Nuclear Science, Kyoto University, Osaka 590-0494, Japan*

Kaoru Tamada − *Institute for Materials Chemistry and Engineering, Kyushu University, Fukuoka 812-0395, Japan;* orcid.org/0000-0003-2618-9924

Takahiro Ochiya − *Department of Molecular and Cellular Medicine, Tokyo Medical University, Tokyo 160-0023, Japan*

Masateru Taniguchi − *The Institute of Scientific and Industrial Research, Osaka University, Osaka 567-0047, Japan;* orcid.org/0000-0002-0338-8755

Complete contact information is available at: https://pubs.acs.org/10.1021/acs.analchem.1c00258

Author Contributions

S.R. and T.Y. contributed equally. S.R., T.Y., M. Tsutsui, T.O., M. Taniguchi, Y.B., and T.K. planned and designed experiments. S.R. and M. Tsutsui fabricated the nanopore devices. S.R., M. Tsutsui, and M. Taniguchi exhibited ionic current measurements. S.R., T.Y., M. Tsutsui, and K.Y. performed data analyses. T.Y., P.P, and Y.B. prepared exosome samples and observed them by TEM. N.K. and D.I. analyzed the velocity of exosomes. Y.K. analyzed the present data by machine learning, and S.R., T.Y., M. Tsutsui, K.T., T.O, M. Taniguchi, Y.B., and T.K. co-wrote the paper.

Notes

The authors declare no competing financial interest.

■ ACKNOWLEDGMENTS

This research is partially supported by the Japan Society for the Promotion of Science (JSPS) through its Funding Program for World-Leading Innovative R&D on Science and Technology and the Japan Society for the Promotion of Science (JSPS) KAKENHI Grant Numbers 15H05417, 16H02091, and 17H04803, and JST PRESTO Grant Numbers JPMJPR17HC and JPMJPR151B, Japan. This work is also performed under the Cooperative Research Program of "Dynamic Alliance for Open Innovation Bridging Human, Environment and Materials".

■ REFERENCES

(1) Ledford, H. *Nature* **2016**, *537*, 288−289.

(2) Loomans-Kropp, H. A.; Umar, A. *npj Precis. Oncol.* **2019**, *3*, No. 3.

(3) Abbosh, C.; Birkbak, N.; Swanton, C. *Nat. Rev. Clin. Oncol.* **2018**, *15*, 577−586.

(4) Cohen, J. D.; Li, L.; Wang, Y.; Thoburn, C.; Afsari, B.; Danilova, L.; Douville, C.; Javed, A. A.; Wong, F.; Mattox, A.; Hruban, R. H.; Wolfgang, C. L.; Goggins, M. G.; Dal Molin, M.; Wang, T.-L.; Roden, R.; Klein, A. P.; Ptak, J.; Dobbyn, L.; Schaefer, J.; Silliman, N.; Popoli, M.; Vogelstein, J. T.; Browne, J. D.; Schoen, R. E.; Brand, R. E.; Wong, H.-L.; Mansfield, A. S.; Jen, J.; Hanash, S. M.; Falconi, M.; Allen, P. J.; Zhou, S.; Bettegowda, C.; Diaz, L. A., Jr.; Tomasetti, C.; Kinzler, K. W.; Vogelstein, B.; Marie Lennon, A.; Papadopoulos, N.; et al. *Science* **2018**, *359*, 926−930.

(5) Lo, T. W.; Nagrath, S. *Nat. Biomed. Eng.* **2017**, *1*, No. 0061.

(6) Kosaka, N.; Yoshioka, Y.; Fujita, Y.; Ochiya, T. *J. Clin. Invest.* **2016**, *126*, 1163−1172.

(7) Fujita, Y.; Yoshioka, Y.; Ochiya, T. *Cancer Sci* **2016**, *107*, 385−390.

(8) Kalluri, R.; LeBleu, V. S. *Science* **2020**, *367*, No. eaau6977.

(9) Dieudé, M.; Bell, C.; Turgeon, J.; Beillevaire, D.; Pomerleau, L.; Yang, B.; Hamelin, K.; Qi, S.; Pallet, N.; Béland, C.; Dhahri, W.; Cailhier, J. F.; Rousseau, M.; Duchez, A. C.; Lévesque, T.; Lau, A.; Rondeau, C.; Gingras, D.; Muruve, D.; Rivard, A.; Cardinal, H.; Perreault, C.; Desjardins, M.; Boilard, É.; Thibault, P.; Hébert, M. J. *Sci. Transl. Med.* **2015**, *7*, No. 318ra200.

(10) Gulei, D.; Irimie, A. I.; Cojocneanu-Petric, R.; Schultze, J. L.; Berindan-Neagoe, I. *Bioconjugate Chem.* **2018**, *29*, 635−648.

(11) Valadi, H.; Ekström, K.; Bossios, A.; Sjöstrand, M.; Lee, J. J.; Lötvall, J. O. *Nat. Cell Biol.* **2007**, *9*, 654−659.

(12) Kosaka, N.; Iguchi, H.; Yoshioka, Y.; Takeshita, F.; Matsuki, Y.; Ochiya, T. *J. Biol. Chem.* **2010**, *285*, 17442−17452.

(13) Szempruch, A. J.; Dennison, L.; Kieft, R.; Harrington, J. M.; Hajduk, S. L. *Nat. Rev. Microbiol.* **2016**, *14*, 669−675.

(14) Madeo, M.; Colbert, P. L.; Vermeer, D. W.; Lucido, C. T.; Cain, J. T.; Vichaya, E. G.; Grossberg, A. J.; Muirhead, D. R.; Rickel, A. P.; Hong, Z.; Zhao, J.; Weimer, J. M.; Spanos, W. C.; Lee, J. H.; Dantzer, R.; Vermeer, P. D. *Nat. Commun.* **2018**, *9*, No. 4284.

(15) Yasui, T.; Yanagida, T.; Ito, S.; Konakade, Y.; Takeshita, D.; Naganawa, T.; Nagashima, K.; Shimada, T.; Kaji, N.; Nakamura, Y.; Thiodorus, I. A.; He, Y.; Rahong, S.; Kanai, M.; Yukawa, H.; Ochiya, T.; Kawai, T.; Baba, Y. *Sci. Adv.* **2017**, *3*, No. e1701133.

(16) Kosaka, N.; Iguchi, H.; Hagiwara, K.; Yoshioka, Y.; Takeshita, F.; Ochiya, T. *J. Biol. Chem.* **2013**, *288*, 10849−10859.

(17) Kosaka, N.; Iguchi, H.; Ochiya, T. *Cancer Sci* **2010**, *101*, 2087−1092.

(18) Hoshino, A.; Costa-Silva, B.; Shen, T. L.; Rodrigues, G.; Hashimoto, A.; Tesic Mark, M.; Molina, H.; Kohsaka, S.; Di Giannatale, A.; Ceder, S.; Singh, S.; Williams, C.; Soplop, N.; Uryu, K.; Pharmer, L.; King, T.; Bojmar, L.; Davies, A. E.; Ararso, Y.; Zhang, T.; Zhang, H.; Hernandez, J.; Weiss, J. M.; Dumont-Cole, V. D.; Kramer, K.; Wexler, L. H.; Narendran, A.; Schwartz, G. K.; Healey, J. H.; Sandstrom, P.; Jørgen Labori, K.; Kure, E. H.; Grandgenett, P. M.; Hollingsworth, M. A.; De Sousa, M.; Kaur, S.; Jain, M.; Mallya, K.; Batra, S. K.; Jarnagin, W. R.; Brady, M. S.; Fodstad, O.; Muller, V.; Pantel, K.; Minn, A. J.; Bissell, M. J.; Garcia, B. A.; Kang, Y.; Rajasekhar, V. K.; Ghajar, C. M.; Matei, I.; Peinado, H.; Bromberg, J.; Lyden, D. *Nature* **2015**, *527*, 329−335.

(19) Yoshioka, Y.; Konishi, Y.; Kosaka, N.; Katsuda, T.; Kato, T.; Ochiya, T. *J. Extracell. Vesicles* **2013**, *2*, No. 20424.

(20) Ryuzaki, S.; Tsutsui, M.; He, Y.; Yokota, K.; Arima, A.; Morikawa, T.; Taniguchi, M.; Kawai, T. *Nanotechnology* **2017**, *28*, No. 155501.

(21) Tsutsui, M.; Hongo, S.; He, Y.; Taniguchi, M.; Gemma, N.; Kawai, T. *ACS Nano* **2012**, *6*, 3499−3505.

(22) Venkatesan, B. M.; Bashir, R. *Nat. Nanotechnol.* **2011**, *6*, 615−624.

(23) Dekker, C. *Nat. Nanotechnol.* **2007**, *2*, 209−215.

(24) Théry, C.; et al. *J. Extracell. Vesicles* **2018**, *7*, No. 1535750.

(25) Tsutsui, M.; Yoshida, T.; Yokota, K.; Yasaki, H.; Yasui, T.; Arima, A.; Tonomura, W.; Nagashima, K.; Yanagida, T.; Kaji, N.; Taniguchi, M.; Washio, T.; Baba, Y.; Kawai, T. *Sci. Rep.* **2017**, *7*, No. 17371.

(26) Tsutsui, M.; Maeda, Y.; He, Y.; Hongo, S.; Ryuzaki, S.; Kawano, S.; Kawai, T.; Taniguchi, M. *Appl. Phys. Lett.* **2013**, *103*, No. 013108.
(27) He, Y.; Tsutsui, M.; Fan, C.; Taniguchi, M.; Kawai, T. *ACS Nano* **2011**, *5*, 5509−5518.
(28) He, Y.; Tsutsui, M.; Fan, C.; Taniguchi, M.; Kawai, T. *ACS Nano* **2011**, *5*, 8391−8397.
(29) Beit-Yannai, E.; Tabak, S.; Stamer, W. D. *J. Cell. Mol. Med.* **2018**, *22*, 2001−2006.
(30) Tsutsui, M.; Yokota, K.; Yoshida, T.; Hotehama, C.; Kowada, H.; Esaki, Y.; Taniguchi, M.; Washio, T.; Kawai, T. *ACS Sens.* **2019**, *4*, 748−755.
(31) Qin, Z.; Zhe, J.; Wang, G. X. *Meas. Sci. Technol.* **2011**, *22*, No. 045804.
(32) Goyal, G.; Darvish, A.; Kim, M. J. *Analyst* **2015**, *140*, 4865−4873.
(33) Vogel, R.; Willmott, G.; Kozak, D.; Roberts, G. S.; Anderson, W.; Groenewegen, L.; Glossop, B.; Barnett, A.; Turner, A.; Trau, M. *Anal. Chem.* **2011**, *83*, 3499−3506.
(34) Kozak, D.; Broom, M.; Vogel, R. Accurate Size, Charge & Concentration Analysis of Liposomes using Tunable Resistive Pulse Sensing *Izon Science White Paper: Izon Science*.
(35) Calò, A.; Reguera, D.; Oncins, G.; Persuy, M.; Sanz, G.; Lobasso, S.; Corcelli, A.; Pajot-Augy, E.; Gomila, G. *Nanoscale* **2014**, *6*, 2275.
(36) Zhang, H.; Freitas1, D.; Kim, H.; Fabijanic, F.; Li, Z.; et al. *Nat. Cell Biol.* **2018**, *20*, 332.
(37) Whitehead, B.; Wu, L. P.; Hvam, M. L.; Aslan, H.; Dong, M.; DyrskjØt, L.; Ostenfeld, M. S.; Moghimi, S. M.; Howard, K. A. *J. Extracell. Vesicles* **2015**, *4*, No. 29685.
(38) Vorselen, D.; van Dommelen, S. M.; Sorkin, R.; Piontek, M. C.; Schiller, J.; Döpp, S. T.; Kooijmans, S. A. A.; van Oirschot, B. A.; Versluijs, B. A.; Bierings, M. B.; van Wijk, R.; Schiffelers, R. M.; Wuite, G. J. L.; Roos, W. H. *Nat. Commun.* **2018**, *9*, No. 4960.
(39) Sun, J.; Zhang, L.; Wang, J.; Feng, Q.; Liu, D.; Yin, Q.; Xu, D.; Wei, Y.; Ding, B.; Shi, X.; Jiang, X. *Adv. Mater.* **2015**, *27*, 1402−1407.
(40) Zhang, L.; Feng, Q.; Wang, J.; Zhang, S.; Ding, B.; Wei, Y.; Dong, M.; Ryu, J. Y.; Yoon, T. Y.; Shi, X.; Sun, J.; Jiang, X. *ACS Nano* **2015**, *9*, 9912−9921.

https://doi.org/10.1021/acs.analchem.1c00258
Anal. Chem. 2021, 93, 7037−7044